


Communication

# Manipulating Orbital Angular Momentum Entanglement in Three-Dimensional Spiral Nonlinear Photonic Crystals

Qian Yu <sup>1</sup>, Chuan Xu <sup>1</sup>, Sixin Chen <sup>1</sup>, Pengcheng Chen <sup>1</sup>, Saiwei Nie <sup>1</sup>, Shijie Ke <sup>1</sup>, Dunzhao Wei <sup>2</sup>, Min Xiao <sup>1,3</sup> and Yong Zhang <sup>1,\*</sup>

- <sup>1</sup> National Laboratory of Solid State Microstructures, School of Physics, and Collaborative Innovation Center of Advanced Microstructures, College of Engineering and Applied Sciences, Nanjing University, Nanjing 210093, China; mg20220151@smail.nju.edu.cn (Q.Y.); dz1734005@smail.nju.edu.cn (C.X.); mg21220179@smail.nju.edu.cn (S.C.); chenpengcheng@smail.nju.edu.cn (P.C.); 181840171@smail.nju.edu.cn (S.N.); 181840105@smail.nju.edu.cn (S.K.); mxiao@uark.edu (M.X.)
- <sup>2</sup> School of Physics, Sun Yat-sen University, Guangzhou 510275, China; weidzh@mail.sysu.edu.cn
- <sup>3</sup> Department of Physics, University of Arkansas, Fayetteville, AR 72701, USA
- \* Correspondence: zhangyong@nju.edu.cn

**Abstract:** We propose and theoretically investigate two-photon orbital angular momentum (OAM) correlation through spontaneous parameter down-conversion (SPDC) processes in three-dimensional (3D) spiral nonlinear photonic crystals (NPCs). By properly designing the NPC structure, one can feasibly modulate the OAM-correlated photon pair, which provides a potential platform to realize high-dimensional entanglement for quantum information processing and quantum communications.

**Keywords:** spontaneous parametric down-conversion; orbital angular momentum; 3D nonlinear photonic crystal



**Citation:** Yu, Q.; Xu, C.; Chen, S.; Chen, P.; Nie, S.; Ke, S.; Wei, D.; Xiao, M.; Zhang, Y. Manipulating Orbital Angular Momentum Entanglement in Three-Dimensional Spiral Nonlinear Photonic Crystals. *Photonics* **2022**, *9*, 504. <https://doi.org/10.3390/photonics9070504>

Received: 10 June 2022

Accepted: 20 July 2022

Published: 21 July 2022

**Publisher's Note:** MDPI stays neutral with regard to jurisdictional claims in published maps and institutional affiliations.



**Copyright:** © 2022 by the authors. Licensee MDPI, Basel, Switzerland. This article is an open access article distributed under the terms and conditions of the Creative Commons Attribution (CC BY) license (<https://creativecommons.org/licenses/by/4.0/>).

## 1. Introduction

Entangled photons play an important role in quantum information sciences. One of the most common methods to generate entangled photons is spontaneous parametric down-conversion (SPDC) [1–3], in which a photon pumped into a nonlinear crystal is converted into a photon pair that satisfies the conservations of momentum and energy [4,5]. Photonic crystals have been widely applied in waveguides, optical encoders, and collimators [6–9]. Inspired by this concept, through fabricating  $\chi^{(2)}$  structures inside a nonlinear crystal (i.e., nonlinear photonic crystal (NPC)), entanglement of down-converted photons with respect to polarization, frequency, space, and orbital angular momentum (OAM) has been experimentally realized [10–12].

One typical OAM-carrying mode is Laguerre-Gauss (LG) mode [13] with its transverse distribution being expressed as

$$LG_p^l(\rho, \varphi) = \sqrt{\frac{2p!}{\pi(|l| + p)!}} \frac{1}{w} \left(\frac{\sqrt{2}\rho}{w}\right)^{|l|} L_p^{|l|} \left(\frac{2\rho^2}{w^2}\right) e^{-\frac{\rho^2}{w^2}} e^{il\varphi}, \quad (1)$$

where  $w$  is the beam waist,  $L_p^{|l|}(x)$  is the associated Laguerre polynomial,  $l$  represents the OAM number, and  $p$  is the radial mode index. OAM has an infinite Hilbert space, which composes a useful basis for high-dimensional entanglement. Applications of high-dimensional OAM entanglement include quantum key distribution and quantum spiral imaging [14–16]. The main method to generate OAM entanglement is SPDC [17–20]. Experimentally, two-photon OAM correlation can be controlled by fabricating different NPC structures to modify the quasi-phase matching (QPM) conditions, or by shaping the pump light [21,22]. The NPC structure can introduce reciprocal lattice vectors to satisfy the QPM conditions to improve the SPDC efficiency [23]. Two-dimensional (2D) NPCs

have been utilized to prepare high-dimensional path-entanglement states [24] or to realize wave-front control [25]. However, it cannot effectively manipulate OAM entanglement through QPM engineering because 2D NPC cannot satisfy the requirements of QPM and wavefront shaping at the same time [26,27]. The recent development of three-dimensional (3D) NPCs via the femtosecond laser direct-writing technique has the potential to solve this problem [28–32]. Here, we theoretically investigate the OAM correlation and the two-photon yield by SPDC processes in 3D spiral NPCs.

### 2. Theory

We consider a type-0 (eee) SPDC process in a 3D spiral NPC. 3D NPCs can be fabricated via femtosecond-laser writing in a z-cut LiNbO<sub>3</sub> crystal. As shown in Figure 1, the second-order nonlinear coefficient distribution in 3D NPC is [33]

$$\chi^2(z, \varphi) = \eta d_{33} \text{sign} \left( \cos \left( \frac{2\pi}{\Lambda} z + l_c \varphi \right) \right) = \eta d_{33} \sum_n F_n e^{in \frac{2\pi}{\Lambda} z} e^{in l_c \varphi} \quad (2)$$

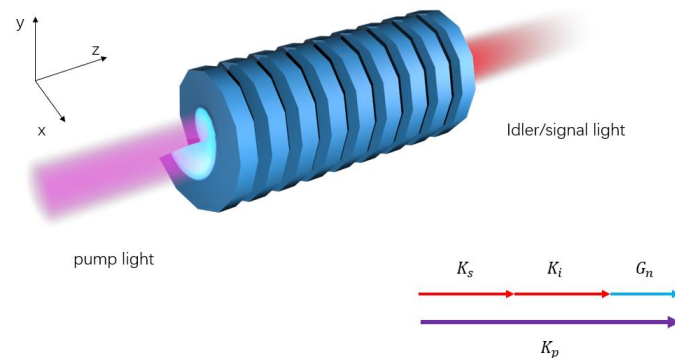


**Figure 1.** Schematic of SPDC in a 3D spiral NPC and the corresponding QPM condition.

Here,  $\varphi = \arctan(y/x)$  is the azimuthal angle,  $l_c$  is the topological charge of the NPC structure,  $\eta$  denotes the modulation depth of nonlinear coefficients,  $d_{33}$  is the nonlinear coefficient of LiNbO<sub>3</sub> crystal, and  $F_n = \frac{2}{n\pi} \sin n\pi D$  are Fourier coefficients corresponding to the reciprocal vector  $G_n = \frac{2\pi n}{\Lambda} z$ .  $D$  is the duty cycle. When  $D = 0.5$ , the maximum Fourier coefficient  $F_1 = 0.635$  can be used by involving the first-order reciprocal lattice vectors  $G_1$ .

The interaction Hamiltonian of the SPDC process is

$$H_I = \epsilon_0 \int dV \chi^2(r) E_p^+ E_s^- E_i^- + h.c., \quad (3)$$

where  $\epsilon_0$  denotes the vacuum permittivity,  $E^+$  and  $E^-$  are respectively the positive and negative conjugate terms of the electric field, the subscripts  $p, s$ , and  $i$  respectively represent the pump, signal, and idler lights, and  $h.c.$  is Hermitian conjugate term. Assuming that the pump light is a normal-incidence monochromatic wave of

$$E_p^+ = E_p e^{i(k_{pz}z - \omega_p t)} f(x, y), \quad (4)$$

where  $E_p$  denotes the amplitude of the pump light,  $f(x, y)$  is the transverse mode of the pump light, and  $k_{pz} = \sqrt{K_p^2 - q_p^2}$ . The first-order Taylor expansion of  $k_{pz}$  is  $k_{pz} = K_p - \frac{|q_p|^2}{2K_p}$ , where  $K_p = n_p \omega_p / c$  and  $q_p$  is transverse momentum that satisfies  $q_p \ll K_p$ .

The down-converted photon can be written as

$$E_j^- = E_j \int d\vec{q}_j \int d\omega_j e^{-i(\vec{k}_j \cdot \vec{r} - \omega_j t)} \hat{a}_j^+ (\vec{q}_j, \omega_j) \quad (5)$$

where  $\hat{a}_j^+(j = s, i)$  denotes the creation operator,  $\omega_j$  is the photon frequency,  $\vec{k}_j = k_j \vec{e}_z + q_j \vec{e}_\rho$ ,  $k_j = K_j - \frac{|q_j|^2}{2K_j}$ ,  $K_j = n_j \omega_j / c$ ,  $\vec{q}_j$  is the transverse component of the wave vector. Considering the  $n^{\text{th}}$ -order reciprocal lattice vector participates in the QPM process, the Hamiltonian can be written as

$$H_I = ALF_n e^{i\frac{\Delta k_z L}{2}} \text{sinc}\left(\frac{\Delta k_z L}{2}\right) \int d\omega_s \int d\omega_i e^{i(\omega_s + \omega_i - \omega_p)t} \times \int d\vec{q}_s \int d\vec{q}_i \iint dx dy f(x, y) e^{i\Delta k_q \rho} e^{inl_c \varphi} \hat{a}_s^+(\vec{q}_s, \omega_s) \hat{a}_i^+(\vec{q}_i, \omega_i), \tag{6}$$

where  $A$  is proportional to  $\eta d_{33}$  and  $L$  is the crystal length. In our scheme, the reciprocal vectors along the  $z$  direction are used to satisfy the QPM condition. We assume a frequency broadening  $\nu_j$  of the down-converted photon, i.e.,  $\omega_j = \Omega_j + \nu_j (j = s, i)$ . Here,  $\Omega_j$  is the central frequency. Considering the energy conservation  $\omega_p = \omega_s + \omega_i$ , we have  $\nu_s = -\nu_i = \nu$ . The phase-matching condition is

$$\frac{2\pi n}{\Lambda} + K_p - K_s - K_i = 0. \tag{7}$$

By expanding wave vectors in  $\nu$ , the longitudinal and transverse phase mismatches can be written as

$$\Delta k_z = -\nu \left( \frac{1}{u_s(\Omega_s)} - \frac{1}{u_i(\Omega_i)} \right) - \nu^2 \left( \frac{d\frac{1}{u_s(\Omega_s)}}{2d\omega_s} + \frac{d\frac{1}{u_i(\Omega_i)}}{2d\omega_i} \right), \tag{8}$$

$$\Delta k_q = -(q_s + q_i), \tag{9}$$

where  $u_j(\Omega_j) (j = s, i)$  is the group velocity at central frequency. Through first-order perturbation theory, the two-photon state wave function can be obtained as

$$|\Psi\rangle = A' LF_n \int d\vec{q}_s \int d\vec{q}_i \int d\nu h(\Delta k_z L) F(\Delta k_q) \hat{a}_s^+(\vec{q}_s, \omega_s) \hat{a}_i^+(\vec{q}_i, \omega_i) |0\rangle, \tag{10}$$

with  $h(\Delta k_z L) = e^{i\frac{\Delta k_z L}{2}} \text{sinc}\left(\frac{\Delta k_z L}{2}\right)$ ,  $F(\Delta k_q) = \iint dx dy f(x, y) e^{i\Delta k_q \rho} e^{inl_c \varphi}$  and  $A' = -\frac{i2\pi A}{\hbar}$ .

Next, we expand the two-photon state by LG eigenstates, i.e.,

$$|\Psi\rangle = \sum_{l_s, p_s} \sum_{l_i, p_i} C_{p_s, p_i}^{l_s, l_i} |l_s, p_s; l_i, p_i\rangle, \tag{11}$$

with

$$C_{p_s, p_i}^{l_s, l_i} = \langle l_s, p_s; l_i, p_i | \Psi \rangle, \tag{12}$$

and

$$|l_s, p_s; l_i, p_i\rangle = \int d\vec{q}_s \int d\vec{q}_i LG_{p_s}^{l_s}(\vec{q}_s) LG_{p_i}^{l_i}(\vec{q}_i) \hat{a}_s^+(\vec{q}_s, \omega_s) \hat{a}_i^+(\vec{q}_i, \omega_i) |0\rangle, \tag{13}$$

where  $LG_{p_j}^{l_j}(\vec{q}_j)$  are the normalized LG modes in  $k$ -space. If considering the incident pump light as an LG mode, we have

$$C_{p_s, p_i}^{l_s, l_i} = A'' LF_n \delta(nl_c + l_p - l_s - l_i) P_{p_s, p_i}^{l_s, l_i} \tag{14}$$

$$P_{p_s, p_i}^{l_s, l_i} = \sqrt{\frac{2p_p! p_s! p_i! (|l_p| + p_p)! (|l_s| + p_s)! (|l_i| + p_i)!}{\pi}} \times \frac{1}{w_p^{|l_p| + |l_s| + |l_i| + 3}} 2^{\frac{|l_p| + |l_s| + |l_i|}{2}} \gamma_s^{|l_s| + 1} \gamma_i^{|l_i| + 1} \times \sum_{j_p=0}^{p_p} \sum_{j_s=0}^{p_s} \sum_{j_i=0}^{p_i} \frac{\left(\frac{\gamma_s}{w_p}\right)^{2j_s} \left(\frac{\gamma_i}{w_p}\right)^{2j_i} \left(\frac{1}{w_p}\right)^{2j_p}}{(|l_s| + j_s)! j_s! (p_s - j_s)! (|l_i| + j_i)! k_i! (p_i - j_i)!} \times \frac{(-2)^{j_p + j_s + j_i}}{(|l_p| + j_p)! j_p! (p_p - j_p)!} Q(\alpha), \tag{15}$$

with

$$Q(\alpha) = \begin{cases} Q_e = \frac{\sqrt{\pi}}{2^\alpha} \frac{\alpha!}{(\frac{\alpha'}{2})!} \left(\frac{1}{\beta}\right)^{\frac{\alpha+1}{2}}, & \alpha \text{ is even} \\ Q_o = \left(\frac{\alpha-1}{2}\right)! \left(\frac{1}{\beta}\right)^{\frac{\alpha+1}{2}}, & \alpha \text{ is odd} \end{cases}, \tag{16}$$

where  $\alpha = |l_p| + |l_s| + |l_i| + 2j_p + 2j_s + 2j_i + 1$ ,  $j_p, j_s, j_i$  are positive integers,  $\beta = \frac{(\gamma_s^2 + \gamma_i^2 + 1)}{w_p^2}$ ,  $\gamma_s = \frac{w_p}{w_s}$ ,  $\gamma_i = \frac{w_p}{w_i}$ , and  $A'' = \frac{2A'}{\pi}$ .  $w_p, w_s$ , and  $w_i$  are respectively the beam waists of the pump, signal, and idler lights.  $|C_{p_s, p_i}^{l_s, l_i}|^2$  represents the joint detection probability of a signal photon at  $|l_s, p_s\rangle$  and an idler photon at  $|l_i, p_s\rangle$

### 3. Results

#### 3.1. Two-Photon OAM Correlation in a 3D Spiral NPC Structure

We illustrate the ability of a 3D spiral NPC structure to manipulate the high-dimensional entanglement state. Note that the traditional 1D NPC cannot be utilized to modulate the OAM correlation. First, we consider the case with  $\gamma_s = \gamma_i = 1, p_p = p_s = p_i = 0$ , and the involved reciprocal lattice vector being  $G_1$ . The topological charge of the spiral NPC structure is set to  $l_c = 1$  and the incident LG mode pump light has  $l_p = 0$ . Because OAM is conserved, i.e.,  $l_s + l_i = l_c + l_p = 1$ , the OAM of the obtained two photons is correlated under a collinear SPDC configuration, satisfying  $l_s = 1 - l_i$  as shown in Figure 2a. Figure 2b shows the result with  $l_c = 2, l_p = 0$ , in which the OAM correlation of the obtained collinear two photons satisfies  $l_s = 2 - l_i$ .

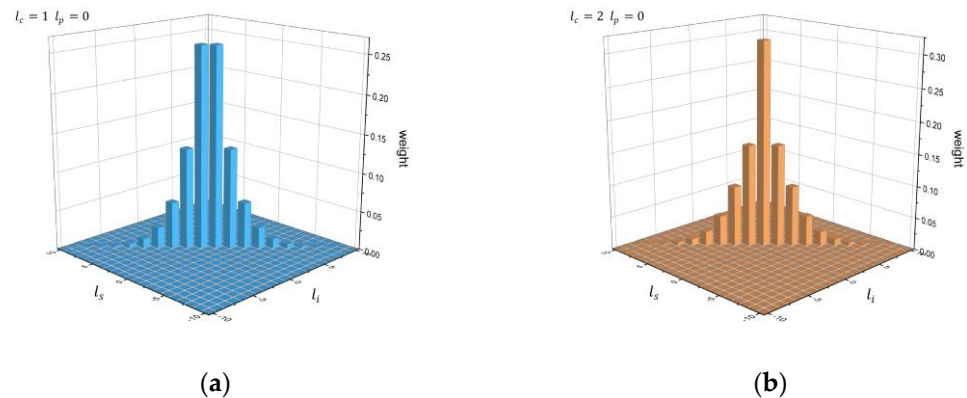


**Figure 2.** The incident light is a Gaussian mode. (a) The normalized spiral spectrum with  $l_c = 1$ . (b) The normalized spiral spectrum with  $l_c = 2$ .

The 3D spiral NPC structure is also able to produce a high-dimensional maximally entangled state. We set the topological charges of the NPC structure and the incident LG mode pump light to  $l_c = 1$  and  $l_p = -1$ , respectively. The OAM conservation during such a SPDC process requires  $l_s + l_i = l_c + l_p = 0$ . We can produce a 3D maximally entangled state of  $|\Psi\rangle = (|-1, 1\rangle + |0, 0\rangle + |1, -1\rangle) / \sqrt{3}$  as shown in Figure 3a. If using  $l_c = -l_p = 2$ , we can produce a four-dimensional maximally entangled state of  $|\Psi\rangle = (|-3, 3\rangle + |-4, 4\rangle + |3, -3\rangle + |4, -4\rangle) / 2$  as shown in Figure 3b.

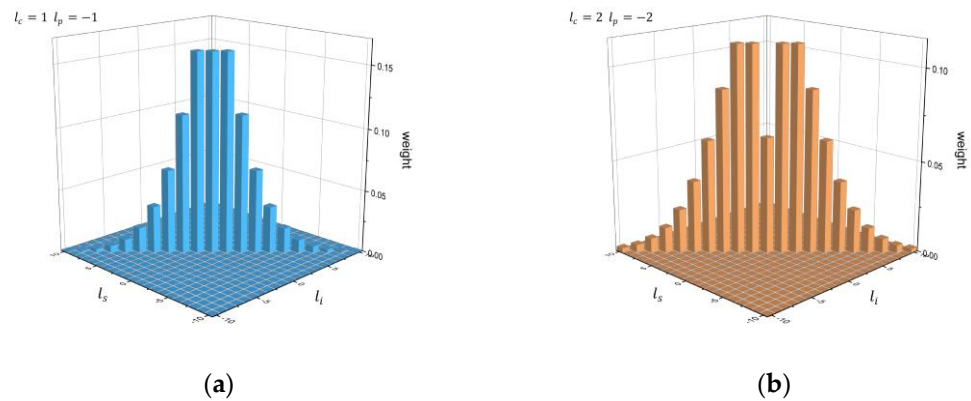


**Figure 3.** A pump light carrying a topological charge opposite to  $l_c$  is used to prepare maximally entangled states. (a) The normalized spiral spectrum with  $l_c = -l_p = 1$ . (b) The normalized spiral spectrum with  $l_c = -l_p = 2$ .

The generation rate of photon pairs can be estimated by the coincidence count rate  $R$ . Here, we use  $E_p^2 = 2P / (\epsilon_0 n_p c S)$ , where  $P$  is the pump power and  $S$  is the transverse area of the pump light. Therefore,

$$R = \frac{\pi \omega_s \omega_i P \Delta \Omega L^2 F_n^2 \eta^2 d_{33}^2}{\epsilon_0 n_p n_s n_i c^3 S}. \tag{17}$$

According to the femtosecond laser direct-writing parameters in [26],  $d_{33} = 27.2 \text{ pm/V}$ ,  $\eta = 0.15$ , and  $F_1 = 0.635$ , corresponding to the first-order reciprocal lattice vector. Assume  $P = 1 \text{ mW}$ ,  $S = 0.01 \text{ mm}^2$ ,  $L = 100 \text{ }\mu\text{m}$ , and  $\Delta \Omega = 1 \text{ nm}$ . Here, we use a 1 nm narrowband filter to guarantee the signal to noise ratio. For QPM condition at  $\lambda_s = \lambda_i = 830 \text{ nm}$ , the structure period is  $\Lambda = 3.05 \text{ }\mu\text{m}$ . Note that these structure parameters are obtainable in experiment [28]. The generation rate is calculated to be 399 pairs/s, which is comparable to the value in a traditional one-dimensional nonlinear photonic crystal [34].

### 3.2. Two-Photon OAM Correlation from the Cascaded 3D Spiral Structure

We consider an  $m$ -segment 3D spiral structure, where each segment carries a different topological charge  $l_c^m$ . The length of each section is  $L_m$ , and the corresponding phase-matching order is  $n$ . The distance between the center of each segment is an integral multiple of the coherence length. Thus, the structure function is

$$f(\varphi, z) = \sum_m \text{sign} \left( \cos \left( \frac{2\pi}{\Lambda} z + l_c^m \varphi \right) \right) = \sum_m \sum_n F_{nm} e^{in \frac{2\pi}{\Lambda} z} e^{in l_c^m \varphi}. \tag{18}$$

The Fourier coefficient  $F_{nm}$  of the  $m^{\text{th}}$  structure can be adjusted by optimizing the duty cycle. Under such a scheme, the generated two-photon OAM state can be described as

$$|\Psi\rangle = \sum_m C_{p_s, p_i}^{l_s, l_i} |n l_c^m + l_p - l\rangle_s |l\rangle_i, \tag{19}$$

with

$$C_{p_s, p_i}^{l_s, l_i} = A'' \sum_m L_m F_{nm} \delta(n l_c^m + l_p - l_s - l_i) P_{p_s, p_i}^{l_s, l_i}, \tag{20}$$

We give two examples. In the first one, two 3D spiral structures of equal lengths are cascaded, carrying topological charges of  $l_c^1 = 2$  and  $l_c^2 = -2$  (Figure 4a). Assume that the first-order reciprocal lattice vectors are involved and the duty cycles are 0.5. Then, the generated two-photon is OAM-correlated, satisfying  $l_s + l_i = \pm 2$ . Figure 4b shows the normalized spiral spectra of photon pairs. In this scheme, the idler photon is projected onto an OAM state of  $|0\rangle_i$  while the signal photon collapses into a superposition of two OAM modes, i.e.,  $(C_2|2\rangle_s + C_{-2}|-2\rangle_s)$  (Figure 4c).

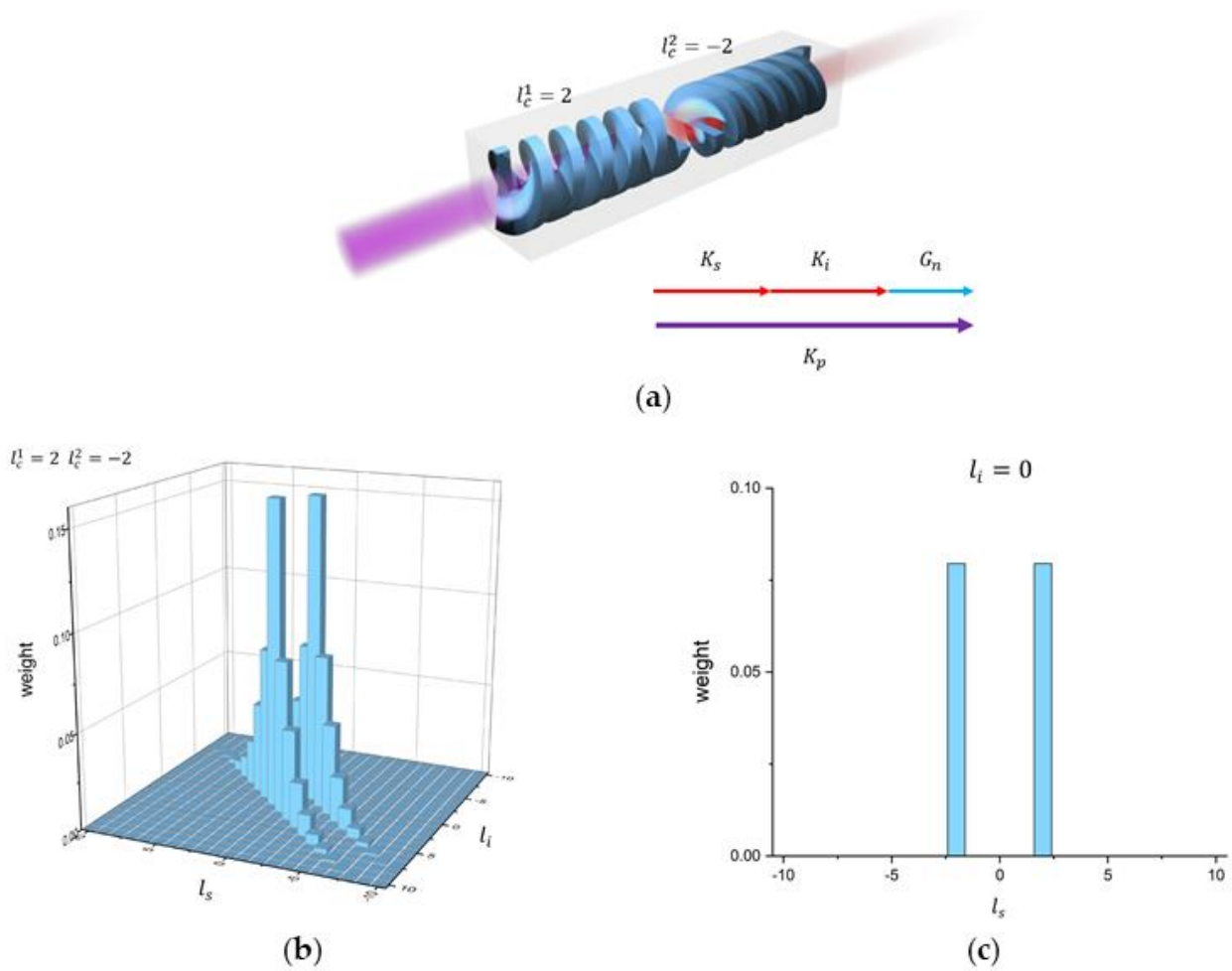


**Figure 4.** (a) The incident light is a Gaussian mode. The NPC sample consists of two spiral structures of opposite topological charges. (b) The normalized spiral spectrum with  $l_c^1 = 2, l_c^2 = -2$ . (c) The spiral spectrum of the signal light when the idler light is projected onto the fundamental mode.

In the second example, we show that the weight in the spiral spectrum can be tuned by adjusting the parameters of each segment. We consider that three spiral structures of equal lengths are cascaded and the topological charges are  $l_c^1 = 2, l_c^2 = 0, l_c^3 = -2$ , respectively. Assume that the first-order reciprocal lattice vectors are involved and the duty cycles are 0.5 (Figure 5a). The generated photon pair is OAM-correlated, satisfying  $l_s + l_i = 0, \pm 2$ . The normalized spiral spectrum is shown in Figure 5c. In this case, the idler photon is projected onto  $|0\rangle_i$ . The signal photon collapses into a superposition of three OAM modes ( $C_2|2\rangle_s + C_0|0\rangle_s + C_{-2}|-2\rangle_s$ ) (Figure 5e). Then we change the length and the duty cycle of each structure to modulate the spiral spectrum. For instance, we double the lengths of the spiral structures with  $l_c^1 = -2, l_c^3 = 2$  and set the duty cycle to 0.25 for the spiral structure with  $l_c^1 = -2$ . The schematic is shown in Figure 5b. The normalized spiral spectrum is shown in Figure 5d. In this case, the idler photon is projected onto  $|0\rangle_i$ . The signal photon collapses into a superposition of three OAM modes ( $C'_2|2\rangle_s + C'_0|0\rangle_s + C'_{-2}|-2\rangle_s$ ) (Figure 5f) with their weights being different from the values in Figure 5e.

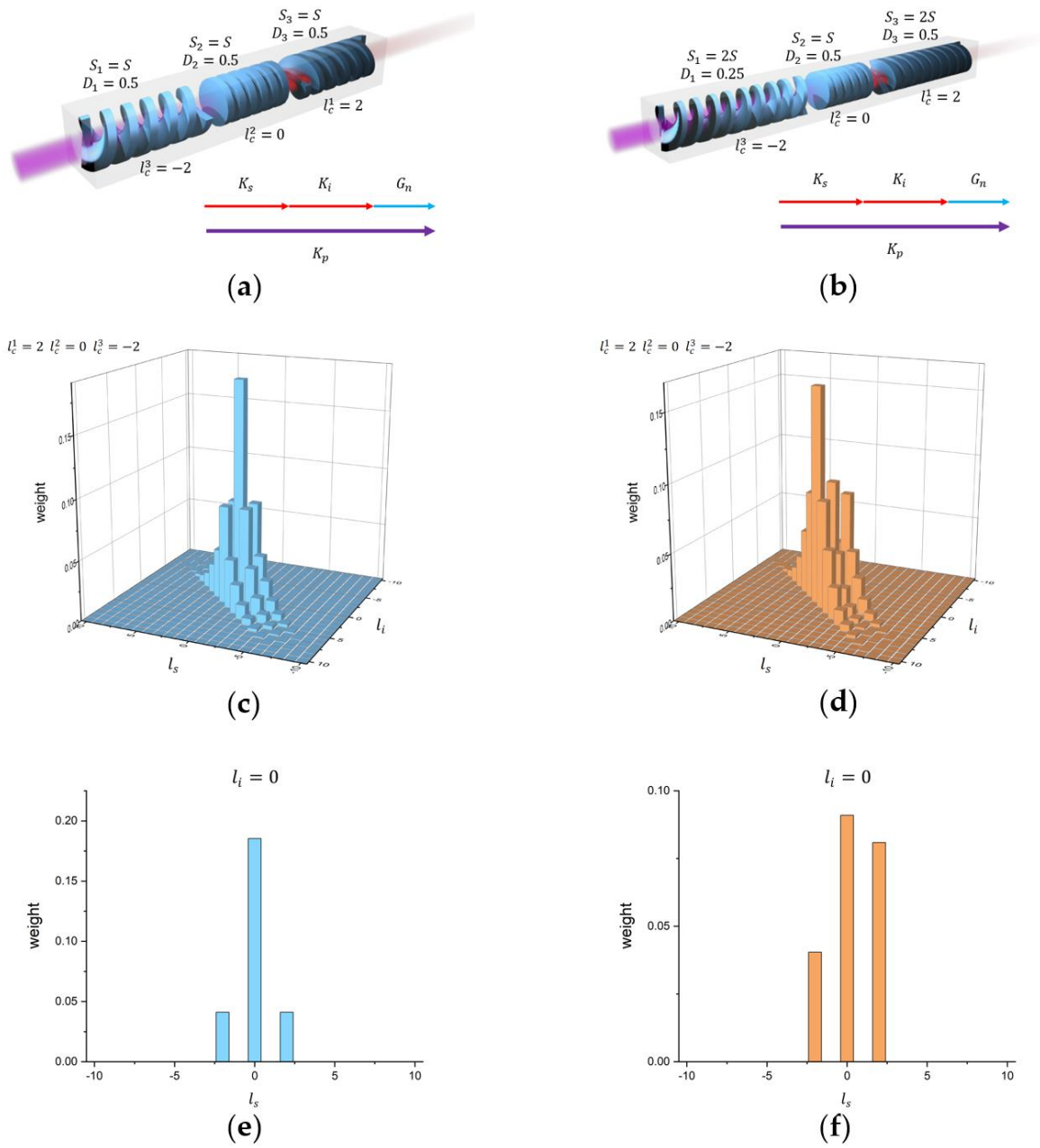


**Figure 5.** (a) The 3D spiral NPC consists of three segments of equal lengths  $S$  carrying topological charges of  $l_c^1 = 2, l_c^2 = 0, l_c^3 = -2$ , respectively. The duty cycles are 0.5. (b) The cascaded spiral NPC with  $l_c^1 = -2, S_1 = 2S, D_1 = 0.25, l_c^2 = 0, S_2 = S, D_2 = 0.5, l_c^3 = 2, S_3 = 2S, D_3 = 0.5$ . (c,d) are the normalized spiral spectra corresponding to (a,b), respectively. (e,f) are the spiral spectra of the signal lights corresponding to (c,d), respectively. Here, the idler light is projected onto the  $|0\rangle_i$  mode.

**4. Discussion**

We have theoretically analyzed the two-photon spiral spectra through SPDC processes in 3D spiral NPCs. The numerical simulations show that the two-photon OAM correlation can be controlled by using various spiral structures or shaping the pump light. In addition, a 3D spiral NPC structure is capable of producing OAM-correlated photon pairs efficiently. Our results pave the way for manipulating high-dimensional OAM entanglement for quantum communication and quantum imaging.

**Author Contributions:** Conceptualization, Q.Y., C.X. and Y.Z.; investigation, Q.Y., C.X., S.C., P.C., S.N., S.K. and D.W.; writing—original draft preparation, Q.Y.; writing—review and editing, Q.Y., C.X. and Y.Z.; supervision, Y.Z. and M.X.; All authors have read and agreed to the published version of the manuscript.

**Funding:** This research was funded by National Key R&D Program of China (2021YFA1400803), the National Natural Science Foundation of China (NSFC) (91950206 and 11874213), Fundamental Research Funds for the Central Universities (021314380220 and 021314380191), and Guangdong Natural Science Funds for Distinguished Young Scholars (2022B1515020067).

**Conflicts of Interest:** The authors declare no conflict of interest.

## References

1. Ou, Z.Y.; Mandel, L. Violation of Bells-Inequality and Classical Probability in a two-Photon Correlation Experiment. *Phys. Rev. Lett.* **1988**, *61*, 50–53. [[CrossRef](#)] [[PubMed](#)]
2. Shih, Y.H.; Alley, C.O. New Type of Einstein-Podolsky-Rosen-Bohm Experiment Using Pairs of Light Quanta Produced by Optical Parametric Down Conversion. *Phys. Rev. Lett.* **1988**, *61*, 2921–2924. [[CrossRef](#)] [[PubMed](#)]
3. Bouwmeester, D.; Pan, J.W.; Mattle, K.; Eibl, M.; Weinfurter, H.; Zeilinger, A. Experimental Quantum Teleportation. *Nature* **1997**, *390*, 575–579. [[CrossRef](#)]
4. Rubin, M.H. Transverse Correlation in Optical Spontaneous Parametric Down-Conversion. *Phys. Rev. A* **1996**, *54*, 5349–5360. [[CrossRef](#)]
5. Rubin, M.H.; Klyshko, D.N.; Shih, Y.H.; Sergienko, A.V. Theory of Two-Photon Entanglement in Type-II Optical Parametric Down-Conversion. *Phys. Rev. A* **1994**, *50*, 5122–5133. [[CrossRef](#)]
6. Haddadan, F.; Soroosh, M. Low-power all-optical 8-to-3 encoder using photonic crystal-based waveguides. *Photonic Netw. Commun.* **2019**, *37*, 83–89. [[CrossRef](#)]
7. Haddadan, F.; Soroosh, M.; Alaei-Sheini, N. Designing an electro-optical encoder based on photonic crystals using the graphene-Al<sub>2</sub>O<sub>3</sub> stacks. *Appl. Opt.* **2020**, *59*, 2179–2185. [[CrossRef](#)]
8. Noori, M.; Soroosh, M.; Baghban, H. All-angle self-collimation in two-dimensional square array photonic crystals based on index contrast tailoring. *Opt. Eng.* **2015**, *54*, 7111. [[CrossRef](#)]
9. Seraj, Z.; Soroosh, M.; Alaei-Sheini, N. Ultra-compact ultra-fast 1-bit comparator based on a two-dimensional nonlinear photonic crystal structure. *Appl. Opt.* **2020**, *59*, 811–816. [[CrossRef](#)]
10. Franson, J.D. Bell Inequality for Position and Time. *Phys. Rev. Lett.* **1989**, *62*, 2205–2208. [[CrossRef](#)]
11. Kwiat, P.G.; Mattle, K.; Weinfurter, H.; Zeilinger, A.; Sergienko, A.V.; Shih, Y.H. New High-Intensity Source of Polarization-Entangled Photon Pairs. *Phys. Rev. Lett.* **1995**, *75*, 4337–4341. [[CrossRef](#)] [[PubMed](#)]
12. Rossi, A.; Vallone, G.; Chiuri, A.; De Martini, F.; Mataloni, P. Multipath Entanglement of Two Photons. *Phys. Rev. Lett.* **2009**, *102*, 153902. [[CrossRef](#)] [[PubMed](#)]
13. Allen, L.; Beijersbergen, M.W.; Spreeuw, R.J.C.; Woerdman, J.P. Orbital Angular-Momentum of Light and the Transformation of Laguerre-Gaussian Laser Modes. *Phys. Rev. A* **1992**, *45*, 8185–8189. [[CrossRef](#)] [[PubMed](#)]
14. Chen, L.; Lei, J.; Romero, J. Quantum Digital Spiral Imaging. *Light: Sci. Appl.* **2014**, *3*, E153. [[CrossRef](#)]
15. Torner, L.; Torres, J.P.; Carrasco, S. Digital Spiral Imaging. *Opt. Express* **2005**, *13*, 873–881. [[CrossRef](#)] [[PubMed](#)]
16. Molina-Terriza, G.; Torres, J.P.; Torner, L. Twisted photons. *Nat. Phys.* **2007**, *3*, 305–310. [[CrossRef](#)]
17. Mair, A.; Vaziri, A.; Weihs, G.; Zeilinger, A. Entanglement of the Orbital Angular Momentum States of Photons. *Nature* **2001**, *412*, 313–316. [[CrossRef](#)]
18. Vaziri, A.; Pan, J.W.; Jennewein, T.; Weihs, G.; Zeilinger, A. Concentration of Higher Dimensional Entanglement: Qutrits of Photon Orbital Angular Momentum. *Phys. Rev. Lett.* **2003**, *91*, 7902. [[CrossRef](#)]
19. Torres, J.P.; Alexandrescu, A.; Torner, L. Quantum Spiral Bandwidth of Entangled Two-Photon States. *Phys. Rev. A* **2003**, *68*, 301. [[CrossRef](#)]
20. Walborn, S.P.; De Oliveira, A.N.; Thebaldi, R.S.; Monken, C.H. Entanglement and Conservation of Orbital Angular Momentum in Spontaneous Parametric Down-Conversion. *Phys. Rev. A* **2004**, *69*, 3811. [[CrossRef](#)]
21. Kovlakov, E.V.; Straupe, S.S.; Kulik, S.P. Quantum State Engineering with Twisted Photons via Adaptive Shaping of the Pump Beam. *Phys. Rev. A* **2018**, *98*, 301. [[CrossRef](#)]
22. Liu, S.; Zhou, Z.; Liu, S.; Li, Y.; Li, Y.; Yang, C.; Xu, Z.; Liu, Z.; Guo, G.; Shi, B. Coherent Manipulation of a Three-Dimensional Maximally Entangled State. *Phys. Rev. A* **2018**, *98*, 2316. [[CrossRef](#)]
23. Torres, J.P.; Alexandrescu, A.; Carrasco, S.; Torner, L. Quasi-Phase-Matching Engineering for Spatial Control of Entangled Two-Photon States. *Opt. Lett.* **2004**, *29*, 376–378. [[CrossRef](#)] [[PubMed](#)]
24. Megidish, E.; Halevy, A.; Eisenberg, H.S.; Ganany-Padowicz, A.; Habshoosh, N.; Arie, A. Compact 2d Nonlinear Photonic Crystal Source of Beamlike Path Entangled Photons. *Opt. Express* **2013**, *21*, 6689–6696. [[CrossRef](#)]
25. Bloch, N.V.; Shemer, K.; Shapira, A.; Shiloh, R.; Juwiler, I.; Arie, A. Twisting Light by Nonlinear Photonic Crystals. *Phys. Rev. Lett.* **2012**, *108*, 3902. [[CrossRef](#)]



26. Lu, L.L.; Xu, P.; Zhong, M.L.; Bai, Y.F.; Zhu, S.N. Orbital Angular Momentum Entanglement via Fork-Poling Nonlinear Photonic Crystals. *Opt. Express* **2015**, *23*, 1203–1212. [[CrossRef](#)]
27. Yang, M.; Jie, T.; Zhao-Xian, C.; Fei, X.; Li-Jian, Z.; Yan-Qing, L. Generation of N00N State with Orbital Angular Momentum in a Twisted Nonlinear Photonic Crystal. *IEEE J. Sel. Top. Quantum Electron.* **2015**, *21*, 225–230. [[CrossRef](#)]
28. Wei, D.; Wang, C.; Wang, H.; Hu, X.; Wei, D.; Fang, X.; Zhang, Y.; Wu, D.; Hu, Y.; Li, J.; et al. Experimental Demonstration of a Three-Dimensional Lithium Niobate Nonlinear Photonic Crystal. *Nat. Photonics* **2018**, *12*, 596–600. [[CrossRef](#)]
29. Xu, T.; Switkowski, K.; Chen, X.; Liu, S.; Koynov, K.; Yu, H.; Zhang, H.; Wang, J.; Sheng, Y.; Krolikowski, W. Three-Dimensional Nonlinear Photonic Crystal in Ferroelectric Barium Calcium Titanate. *Nat. Photonics* **2018**, *12*, 591–595. [[CrossRef](#)]
30. Wei, D.; Wang, C.; Xu, X.; Wang, H.; Hu, Y.; Chen, P.; Li, J.; Zhu, Y.; Xin, C.; Hu, X.; et al. Efficient Nonlinear Beam Shaping in Three-Dimensional Lithium Niobate Nonlinear Photonic Crystals. *Nat. Commun.* **2019**, *10*, 4193. [[CrossRef](#)]
31. Wang, T.; Chen, P.; Xu, C.; Zhang, Y.; Wei, D.; Hu, X.; Zhao, G.; Xiao, M.; Zhu, S. Periodically Poled Linbo3 Crystals from 1d and 2d to 3d. *Sci. China Technol. Sci.* **2020**, *63*, 1110–1126. [[CrossRef](#)]
32. Zhang, Y.; Sheng, Y.; Zhu, S.; Xiao, M.; Krolikowski, W. Nonlinear Photonic Crystals: From 2d to 3d. *Optics* **2021**, *8*, 372–381. [[CrossRef](#)]
33. Bahabad, A.; Arie, A. Generation of Optical Vortex Beams by Nonlinear Wave Mixing. *Opt. Express* **2007**, *15*, 17619–17624. [[CrossRef](#)] [[PubMed](#)]
34. Gong, Y.-X.; Xie, Z.-D.; Xu, P.; Yu, X.-Q.; Xue, P.; Zhu, S.-N. Compact source of narrow-band counterpropagating polarization-entangled photon pairs using a single dual-periodically-poled crystal. *Phys. Rev. A* **2011**, *84*, 3825. [[CrossRef](#)]